Science of the Total Environment 908 (2024) 168425

Contents lists available at ScienceDirect

Science of the Total Environment

journal homepage: www.elsevier.com/locate/scitotenv

Structural analysis and characterization of biosolids. A case study of biosolids from wastewater treatment plants in Western Greece

A.E. Kanteraki [a,*], E.A. Isari [a], I. Zafeiropoulos [a], S. Cangemi [c], A. Bountla [b], I.K. Kalavrouziotis [a]

[a] School of Science and Technology, Hellenic Open University, 26 222 Patras, Greece
[b] Soil and Water Resources Institute, Hellenic Agricultural Organization - DEMETER, Thessaloniki 57001, Greece
[c] Centro Interdipartimentale di Ricerca CERMANU, Università di Napoli Federico II, Via Università 100, 80055 Portici, Italy

HIGHLIGHTS

- Comparative structural analysis of BS from wastewater treatment plants in Greece
- FTIR detailed characterization of BS
- SiO_2 was detected as the main crystalline material.
- Fe, Zn and MN are the dominant traced heavy metals in BS.

GRAPHICAL ABSTRACT

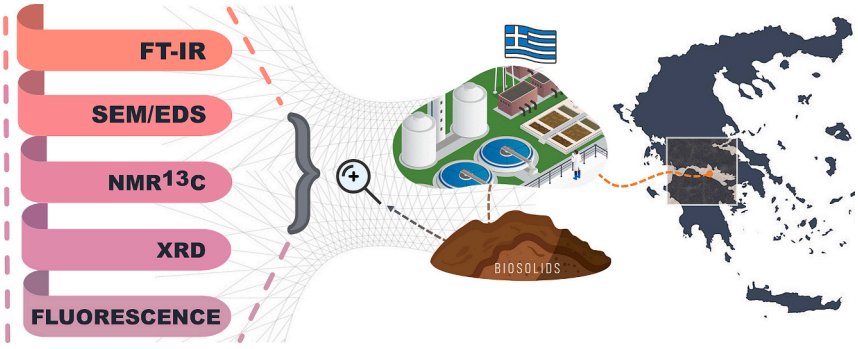

ARTICLE INFO

Editor: Damià Barceló

Keywords:
Biosolids
SEM
XRD
NMR
Structural characterization
Heavy metals

ABSTRACT

The great interest of modern societies in the reuse of wastes opens up new horizons in the field of wastewater, as well. In particular, the treated sludge resulting from a Wastewater Treatment Plant (WWTP) is dealed with a new perspective in the context of circular economy. The aim of this study is the characterization of its complex matrix, and the evaluation for reuse. Biosolids (BS) collected from four urban WWTPs in the Western region of Greece i.e. Agrinio (AG), Amaliada (AM), Aegio (AE) and Itea (IT). Analytical and spectroscopical methods namely TGA, ICP-OES, Fluorescence, SEM/EDS, XRD, FT-IR and NMR were the means that served this purpose. SEM along with XRD proved the amorphous nature of BS. The dominant metals detected in the samples are: Fe, Zn, Mn, with concentrations which meet the guidelines included in 86/278/EEC Directive. The inorganic load is of great importance, along with their humic acid content, adding value at the samples as fertilizers. BS appeared to be rich in organic matter with long aliphatic chains and numerous functional groups, as capturedin FT-IR spectra. The applied methods form an analytical protocol of the BS mapping, highlighting its potential as a material to be utilized in agriculture.

Abbreviations: WWTP, Wastewater treatment plants; WW, Wastewater; SS, Sewage Sludge; BS, Biosolids.

* Corresponding author.
E-mail address: kanteraki.alkistis@ac.eap.gr (A.E. Kanteraki).

https://doi.org/10.1016/j.scitotenv.2023.168425
Received 5 September 2023; Received in revised form 26 October 2023; Accepted 6 November 2023
Available online 7 November 2023

1. Introduction

Wastewater (WW) treatment, which includes physical, chemical, biological and currently advanced oxidation methods, is the process of removing contaminants from WW in order to handle the produced by-products of water and sludge in a more sustainable way (Demirbas et al., 2017). In this context, treated water is released to the natural recipient (i.e. lake, open sea) or used for irrigation (Pollice et al., 2007). On the contrary, sewage sludge (SS), which is the solid residues of the treatment, is not further processed and ends up either for storage or landfill, both of which are considered as obsolete methods (Paz-Ferreiro et al., 2018). Sludge which has undergone further treatment such as aerobic or anaerobic digestion, dewatering via centrifugation, disinfection, thermal or chemical conditioning (Chaudhary and Y. K. G., 2021; Wang et al., 2018), sanitation via advanced oxidation treatment processes; like cold plasma (Svarnas et al., 2020), and has met standards required for beneficial use, is known by the term Biosolids (BS) and can be used as fertilizer in agriculture (Aguilera et al., 2007; Silveira et al., 2007). Specifically, BS are organic solid products rich in nutrients (Kanteraki et al., 2022), which according EPA's "A Plain English Guide to the EPA Part 503 Biosolids Rule", can be recycled and used as fertilizer in agriculture or soil conditioner or be discarded (Walker et al., 1994), once specific limits are met and practices are implemented to protect public health and environment from chemical and microbial pollutants embedded in their matrix.

The constant expansion of industrialization and population growth, has directly caused the generation of huge amounts of BS, which must be handled in a more rational way in the context of agricultural, economic and environmental sustainability (Collivignarelli et al., 2019; Kalavrouziotis and Koukoulakis, 2016).

The latest decades, in the European Community, more than 45 % of produced BS is reported to be used as soil amendments in agriculture (Sharma et al., 2017). In Greece, the disposal guidelines of BS are regulated by the Directive 86/278/EEC (European Union, 1986) which sets specific concentrations limits of heavy metals, and mandates frequent monitoring of other values such as of pH, dry matter, nitrogen and phosphorus. This direction of reuse appears to be optimistic and the most beneficial option, since BS due to their inorganic and organic load can improve the physical properties of soil and prevent the use of chemical fertilizers (Kalavrouziotis, 2016; Silveira et al., 2003). The Directive has been in force for over 30 years and, although major milestones have been achieved, yet pollutants are still emerging that need to be tackled and included or addressed by the current rules. The scientific community and government parties are aware of the growing evidence of contaminants of emerging concern, including micro-pollutants such as pharmaceuticals and micro-plastics, as an increasingly important issue. To address this, the Commission on 2022 proposed an update of the Directive taking these issues into account. Kelly et al. (2020) reported the complex nature of BS. Physical, chemical, microbiological parameters, organic micro-pollutants and heavy metals, that are contained in BS (Collivignarelli et al., 2020) can reflect the quality of their matrix (Kanteraki et al., 2022).

The inorganic and organic load, the percentage of aromaticity, physicochemical characteristics, and their ability to bind with nutrients define the suitability of BS in agriculture (Mossa et al., 2017). Beyond this context of reuse, the possible use of BS as raw material for biochar production derives from the good knowledge of the porosity, moisture, elemental composition and thermal behavior (Paz-Ferreiro et al., 2018). Additionally, BS open up a new chapter in the construction industry as a raw material for the production of bricks, cement, concrete mix and aggregates. Thus, the formation of a product of equal mechanical properties, require the knowledge of BS' particles size distribution, morphology, moisture content, chemical and mineral composition (Mymrin et al., 2019). Consequently, having a detailed structural analysis, is possible to intervene in their production process, changing and improving their characteristics and making them suitable for their future utilization.

So far, systematic risk assessment studies of the potential environmental impacts caused by reusing BS in agriculture, have extensively been analyzed (Smith, 2008). A qualitative description of the actual risk of components such as potentially toxic elements, organic contaminants, pathogens and nutrients, against potentially impacted environmental parameters i.e. human and animal health, cop yields, soil fertility, quality of surface and ground waters, have been also ascribed. Main and widely measured indexes of BS are pH, conductivity, Total Organic Carbon and Volatile Solids since they are indicators of agricultural interest that should be taken into account, because they can affect soil quality and functionality (Medina-Herrera et al., 2020). Other less examined parameters are the texture mechanical analysis via Bouyoucos method (Garrido et al., 2005) and $CaCO_3$ concentration with Bernard calcimeter test (Aadraoui et al., 2017). The understanding of BS molecular structure can be achieved via spectroscopic techniques such as FT-Raman, NMR, UV–Vis, XRD, ICP and EDS (Onchoke et al., 2018). Scientific community has directed their effort towards examining one or two techniques at a time, mainly oriented to SS (Chiu and Tian, 2011; Kowalski et al., 2018; Li et al., 2022; Martínez et al., 2012). Therefore, the interpretation of spectra is still challenging, due to the lack of data dedicated to BS.

The proposed novelty of the present study is the holistic approach of BS characterization, combining analytical techniques to enhance the understanding the complex matrix of this always up-to-date topic. To the best of our knowledge no systematic investigations have been reported in the context of the characterization of BS from WWTPs in Greece and quite a few have been conducted worldwide. Hence, this collective case study evaluated the physical, chemical, and spectroscopic properties of BS which has been produced and collected from four (4) municipal WWTPs in the wider area of Western Greece, presenting data of particular importance for the quantitative and qualitative analysis of BS, contributing to literature's database.

2. Materials & methods

2.1. Study area

BS were sampled during spring of 2022 from four (4) WWTPs in Western Greece (Fig. S1) that receive residential, hospital, commercial, industrial and septic tanks' WW. Key information such as population, geographical coordinates and treatment processes are presented in Table S1. BS derived from aerobic digestion processes and further dewatered and thickened by centrifugation and pressed band filtration systems, by belts pressing the sludge slightly enough to push water through a permeable media away.

2.2. Sample collection and preparation

During March, April and May of 2022, BS samples were collected every 15 days from AM, AG, AE and IT WWTPs following the guidelines of the sludge sampling protocol (DEP, 2021; Office Of Water, 1969). Approximately 5 kg of each sample was taken right after the pressure bands on the first day of the final process and transferred to the laboratory sealed, in sample containers. Part of the raw sample was stored in wide mouth glass containers filled to capacity with Teflon-lined screw-cap top (Mattigod and Zachara, 1996) in the refrigerator at 4 °C for physicochemical analysis, and the remaining amount was dried overnight in oven at 105 °C, pulverized and sieved with 1 mm sieve. The samples for the spectroscopic analysis were stored in polyethylene bottles in desiccator. The physicochemical analysis carried out within five days to avoid variances in values such as moisture (Ho et al., 2010b), volatile solids and pH (DEP, 2021). This timeframe (Hossner, 2018) offers safe accuracy among replicates before mold growth. Three (3) replicates of each sample were analyzed, by the chosen techniques and representative results of each one was chosen. Significant differences were not found neither among replicates of each sample nor between each sampling day.

2.3. Sample characterization

2.3.1. Physicochemical analysis

The pH of the initial samples was recorded in a suspension of BS and deionized water, at a ratio of 1:3 with a Mettler Toledo MP230 instrument. Electrical conductivity (EC) was measured in a 1:3 solid-to-water suspension with a HANNA HI 993310 conductivity meter (Ho et al., 2010a; Jan et al., 2018; Thomas, 2018). Moisture content of each sample was determined by the difference in weight before and after the drying cycle at 105 °C for 1 h. Total Organic Carbon (TOC) was calculated with the Shimadzu SSM-5000 A analyzer. Total Volatile Solids (TVS) were calculated with the Loss on Ignition (LOI) method by comparing the weight of the dried samples after heating at 550 °C for 3 h.

2.3.2. Thermogravimetric analysis (TG/DTG)

TG analysis of the samples was carried out under nitrogen atmosphere at flow rate of 200 mL min^{-1} in a PerkinElmer Diamond Thermogravimetric/ Differential Thermal Analyzer (TG/DTA). About 10 mg of powdered sample was placed in a platinum pan at room temperature. Initially the temperature was raised at 100 °C and kept constant at this value until moisture removal and weight stabilization. After this step, the temperature was increased from 100 °C to 600 °C at a heating rate of 10 °C min^{-1} and remained at this temperature for 1 min.

2.3.3. Inductively Coupled Plasma Optical Emission Spectroscopy (ICP-OES)

10 g of pulverized sample of BS were weighted and 20 mL of the DTPA extraction solution [0.005 M diethylenetriaminepentaacetic acid, 0.01 M calcium chloride ($CaCl_2$), and 0.10 M triethanolamine adjusted to pH 7.3] was prepared for the extraction of micronutrients (Lindsay and Norvell, 1978). The duration of the extraction was 2 h and the extracts were filtered through Whatman No. 2 filter paper. The filtrates were analyzed by ICP-OES (Perkin Elmer Avio 220 Max) in certain wavelengths which are detailed mentioned at S.2.3.3.

2.3.4. Fourier-Transform Infrared Spectroscopy (FT-IR)

In order to classify the nature of functional groups of BS, IR spectra of the four WWTPs' samples obtained using Fourier Transform Infrared (FT-IR) spectrophotometer under ambient conditions. FT-IR spectra were obtained with PerkinElmer 100. Approximately 1 mg of powdered BS was grounded and agitated with 100 mg KBr (spectroscopy grade). The pill (1 mm thickness, 13 mm diameter) was formed by pressing the milled matrix using a hydraulic bench press. Spectra collected over the frequency range of 400–4.000 cm^{-1} region on a sampling pad with a 2 cm^{-1} resolution and corrected against air as background via Perkin Elmer Spectrum 100 spectrometer. Spectra finally processed using Spectrum software.

2.3.5. X-Ray Diffraction (XRD)

Bruker AXS D8 Advance diffractometer (XRD) was used to characterize the crystallinity. Part of the air-dried BS samples were grounded into a homogenized smooth powder and then carefully placed on a Bruker AXS D8 Advance diffractometer's sample holder. Patterns of the fine powdered samples were performed in the 2θ range of 5° - 70° for determining the crystal structure. Diffractometer was configured with a Cu K_α radiation (40 kV, 40 mA, $\lambda = 1.5418$ Å) using a Ni filter at scanning speed of 2°/min. Spectra initially evaluated via diffraction file of the Bruker AXS DIFFRAC.EVA software (DIFFRAC EVA, n.d.). This software was also used to smooth the spectra, and to determine the diffraction peaks positions and intensities. Owing to the complex nature of the samples, the subset of Crystallography Open Database was queried. Crystallinity and crystallite size were also determined by this software.

2.3.6. Cross Polarization (CP) Magic-Angle Spinning (MAS) NMR ^{13}C

The molecular structure of the organic matter of BS was determined by Nuclear Magnetic Resonance (NMR) spectroscopy. The solid state ^{13}C CPMAS NMR spectra were acquired with a Bruker AV300 instrument equipped with a 4 mm wide-bore MAS probe. The powdered samples were filled in 4 mm zirconium rotors with Kel-F caps. The operational parameters were set as follows: a rotor spin rate of 10,000 Hz, 2 s of recycle time, 1 ms of contact time, 30 ms of acquisition time and 4000 scans.

NMR spectra were processed using MestreNova software version 4.1.2 (Mestrelab Research S.L., Madrid, Spain) to evaluate the contribution of each functional group by splitting the overall chemical-shift range into the main resonance intervals, corresponding to organic components following literature (Table S4). The relative percentage contents of different C functional groups were determined by the integration of the peak areas within each spectrum (Chiu and Tian, 2011).

2.3.7. Three-dimensional Excitation-Emission (EEM) Matrix fluorescence spectrophotometer

Fluorescence spectra were obtained from the Dissolved Organic Matter (DOM) of BS. DOM derived from a ratio of 5 g of dry powdered sample with 50 mL H_2O after overnight equilibration at room temperature (~20 °C) and centrifugation at 4.000 rpm for 10 min. The supernatant was then filtered through a 0,22 μm nitrocellulose membrane filter and the pH was adjusted with 0,05 M NaOH solution to approximately 7,3. The EEM spectra obtained by Agilent Cary Eclipse Fluorescence Spectrophotometer equipped with the Cary WinFLR software. The emission and excitation slits were set to 5 and 10 nm, respectively. The constant scale setting was chosen for each sample in such a way that the maximum fluorescence intensity of the most intense peak in each spectrum could approach 90 % of the relative intensity (Senesi et al., 1991). In this way, the relative intensity for the various samples can then be calculated with comparable values. To obtain the EEM, the excitation wavelengths adjusted from 220 to 600 nm and the scanning emission wavelength modulated between 280 and 800 nm with a step of 5.0 nm.

2.3.8. Scanning Electron Microscopy/Energy Dispersive X-ray Spectrometer (SEM/EDS)

SEM equipped with EDS was used for the surface morphology of BS and their chemical composition. Powdered samples were applied on top of the steel stubs and coated with gold using BALTEC MED 020 sputter coater to avoid electron-charging of BS. SEM micrographs recorded with a JEOL 6300 (JEOL GmbH, Freising, Germany) at 15 kV at 800× and 2.000× magnification level. The EDS spectrum (OXFORD, Link Penta-Fet) (inlet) allowed the element distribution of the samples.

3. Results & discussions

In preface to the results that will be presented in detail, it is considered important to emphasize the need to manage BS in a more sustainable way. In the context of the circular economy, more attention should be given to the various ways of using BS that are suitable as soil amendments, eliminating environmental risks such as eutrophication, while maximizing the benefits of their reuse (Medina-Herrera et al., 2020). Thus, mapping techniques and methods that can give us information about this complex organic matter, is meaningful.

3.1. Physicochemical properties of BS

The physicochemical characteristics of BS are summarized in Table S2. The recorded pH values ranged among 6,8 and 7,4. In other studies, using samples of BS from urban WWTPs, pH mean values have been reported equal to 6,9 ± 0.1 (Tapia et al., 2010). Conductivity values showed significant observed differences; varying between 70 μS

cm^{-1} and 1.150 μS cm^{-1} were observed. The percentages of moisture ranged from 60 to 70 % which is high as expected due to the nature of the samples. Values of TOC did not differ significantly and were comparable to other reports (i.e. 36–57 %) (Medina-Herrera et al., 2020). Rowell et al. (2001) have recorded even lower values (31–35 %). Volatile solids ranged from 76 % to 92 % which was in line with the findings of literature (i.e. 86 %) (Vochozka et al., 2016). These data from the measured parameters showed minimal differences among the BS, with the exception of conductivity, which was an indication of geographic location of the samples. In particular, the EC of BS sample from the WWTP of AE showed the highest value, which is probably due to the high salinity of the coastal area (Laidlaw et al., 2015). Overall, however, the results of the physicochemical analysis were in accordance with the guidelines of the Directive of 86/278/EEC guidelines (European Union, 1986) meeting the initial prerequisites for their assessment as materials suitable for reuse.

3.2. Thermal analysis of BS

The TG analytical technique has been extensively used to study the pyrolysis behavior of various types of biomass (e.g. lignocellulosic materials, BS, polymeric materials, meat waste, etc.). It has been found that the effect of pyrolysis temperature, heating rate and biomass composition can be studied in detail by TG analysis (Patel et al., 2018).

The present TG/DTG analysis focused on the second (180 to 350 °C) and third (350 to 600 °C) stages of pyrolysis, aiming to study the two fractions of the organic matter contained in the BS, the volatile fraction and the difficult to biodegrade part. The TGA/DTG graph of sample IT (Fig. 1) is presented in the current study as a representative result of the BS TG analysis. The samples having first been dehydrated, were not tested for Stage I (25 to 180 °C) pyrolysis. For this reason, the selected temperature range was 100 to 600 °C.

The DTG curve of BS showed a strong peak at the volatilization stage, between 300 and 310 °C, which is probably due to the degradation of proteins and carboxyl groups to carbon dioxide (CO_2) to a greater extent and to a lesser extent to carbon monoxide (CO) and volatile organic compounds (Gao et al., 2014). The percentage of mass loss at this stage varies from 25 to 34 %, because of the pyrolysis of hydrocarbons and dead microorganisms, which are the most readily biodegradable fraction of volatile organic matter of BS. The majority of these organic components tend to decompose in the volatilization phase producing bio-gas and bio-oil. In the third stage, a "shoulder" appears between 440 and 450 °C in the samples, which is probably due to the degradation of higher molecular weight compounds to methane (CH_2) and light volatile compounds (Chen and Jeyaseelan, 2001). A lower percentage of mass loss rate of 18 to 21 % was observed at Stage III, due to the degradation of the smaller fraction of lignin, macromolecular humic compounds, as well as, synthetic organic polymers in the BS matrix.

The TG analysis did not reveal different thermal behavior between the BS samples that were collected from the different WWTPs. Through the analysis, the opinion that BS are organic protein-rich materials was reinforced. Their organic matter ranged from 50 to 60 % and the existence of humic substances made them value-added products for land application.

3.3. Metal concentrations in BS

The dominant metals present in the studied BS were Fe, Mn, Zn, Ni and Cu. In smaller quantities Cd, Co, Cr and Pb were also present. Table 1 shows the concentrations of trace metals in the measured concentrations and the limits that are regulated by the Directive 86/278/EEC.

Initially, the values do not exceed the permissible limits of metals in the sludge according to the regulated limits of heavy metals in BS for agricultural application. The only exception being Cu in the AG. Variation in concentrations between WWTPs, may be due either to the location of the plant, the nature of the influents or the treatment processes. In a more general context, the values follow the same trend compared to a corresponding studies that have taken samples from units that fit the above profile of the above (Demitrelos et al., 2022; Giannakopoulos et al., 2017).

With minor variations, all the units followed this order: Fe > Zn > Mn > Cu > Pb > Ni > Co > Cd > Cr. The high value of Mn recorded in the IT is noteworthy (213 mg kg^{-1}) and is the only record that breaks the

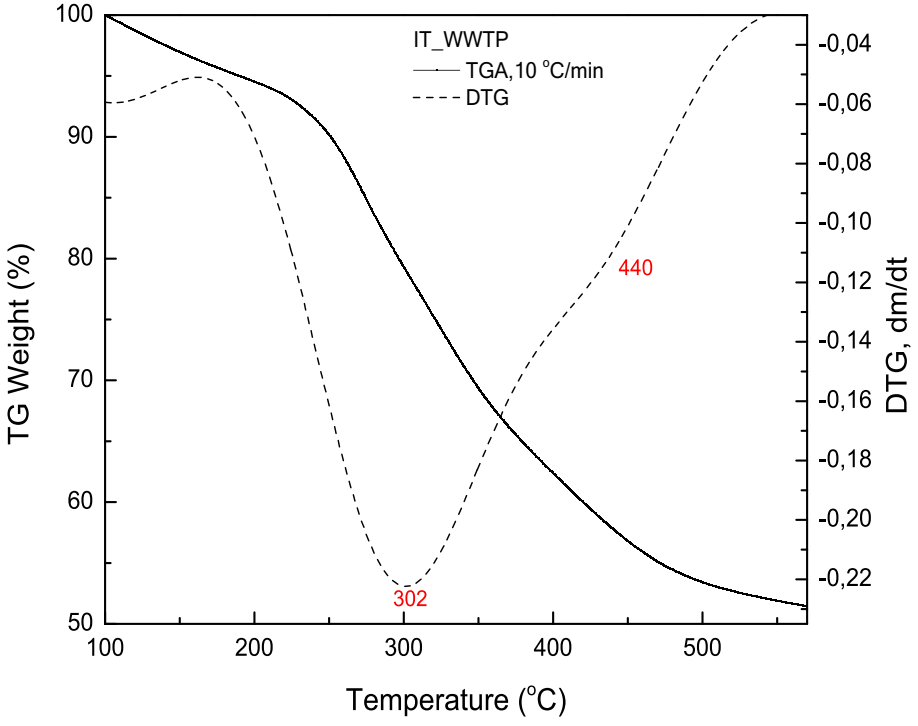

Fig. 1. TG/DTG graph of IT sample.

Table 1
Elemental composition of BS from WTTPs.

	Fe	Zn	Mn	Cu	Cd	Co	Cr	Ni	Pb
	mg kg^{-1}								
AG	245,5	205,7	176,1	151,9	0,4	1,0	0,3	6,9	18,7
AM	554,0	65,3	27,4	12,0	0	0,4	0,5	5,7	14,9
AE	671,3	117,9	42,8	17,6	0	0,4	0,4	7,3	18,0
IT	392,4	111,7	213,3	10,6	0,1	0,9	1,1	6,6	11,7
DIRECTIVE 86/278/EEC	–	150–300	–	50–140	1–3	–	–	30–75	50–300

Fe > Zn > Mn sequence. It also appears that Cd, Co, Cr, Ni, Pb follow similar trend of concentrations.

3.4. Identification of functional groups of BS

The identification of the functional groups present in BS was carried out via FT-IR spectroscopic analysis (Fig. 2). A detailed matching of the wavenumbers of samples' detected peaks with the characteristic bands recorded from the literature is listed in the Table 2.

The transmittance peaks located between 3650 and 3250 cm^{-1} [#1] of the FT-IR spectra indicate the existence of hydrogen bonding in OH group (Smidt and Meissl, 2007). The OH groups can be free or belong to carboxylic acids, phenols, polysaccharides or other saturated aliphatic species (K. Wang et al., 2013). The absorption bands in [#2], [#3] and [#4] are attributed to aliphatic methylene groups and assigned to fats and lipids. Lipids are an important fraction of BS that could affect the water holding capacity of amended soils, their structural stability and the biodegradation-moisture balance in soils (Grube et al., 2006). Dominant FT-IR absorption peaks of the various sample fractions were at the following wavelengths: 3432–3420 cm^{-1} (H-bands, OH groups), 2962–2955 cm^{-1} (C—H stretching from –CH_2 and –CH_3), 1466–1424 cm^{-1} (distortion of C—H groups from CH_2 or CH_3), 1247–1235 cm^{-1} (P═O, C-O-C stretching and amides III).

Several intense characteristic bands [#6, #8, #11] can be attributed to functional groups present in proteins and polysaccharides. Two bands of weak intensity around 1545 cm^{-1} and 1655 cm^{-1} are of protein origin (Amide II and Amide I respectively). A peak at 1577 cm^{-1} [#7] detected only in the AM matter and is attributed possibly to an ammonium bending vibration. Some bands were also observed in the "fingerprint" area. Previous studies have shown that the IR spectra of SS differ from other organic wastes with an intense, broad, typically asymmetric absorption band around 1034 cm^{-1}, such as those shown in [#11] and attributed to the presence of phosphate-containing minerals and silicates.

Whereas, the vibration at 800 cm^{-1} may be the indication of C—O stretching associated with carbonate and/or silica, as observed from FT-IR results of vermicomposts by Carrasquero-Durán and Flores (2009) and Ravindran et al. (2008) (Carrasquero-Durán and Flores, 2009; Ravindran et al., 2008).

Small band at 874 cm^{-1} and other peaks from 700 to 400 cm^{-1} are also related to $Ca(OH)_2$ present in SS. The weak band around 535 cm^{-1} could be attributed to PO_4^{3-} which may be related to phosphate compound in the activated sludge. In general, vibrations smaller than 1000 cm^{-1} are the result of functional groups containing sulfur and phosphorus (Flores-Álvarez et al., 2011).

Summarizing all the above mentioned findings, analysis of the IR spectra showed the presence of numerous functional groups, through the various peaks, following the trend of corresponding spectra of BS and SS (Flores-Álvarez et al., 2011; Kang et al., 2007; Medina-Herrera et al., 2020; Onchoke et al., 2018). The spectra of the four BS of different origins were qualitatively similar. This can be attributed to the common origin of BS and that the WWTPs' processes are identical with minor modifications. Also, the SS stabilization process is shown to produce BS of stable structure (Medina-Herrera et al., 2020). The relative intensity

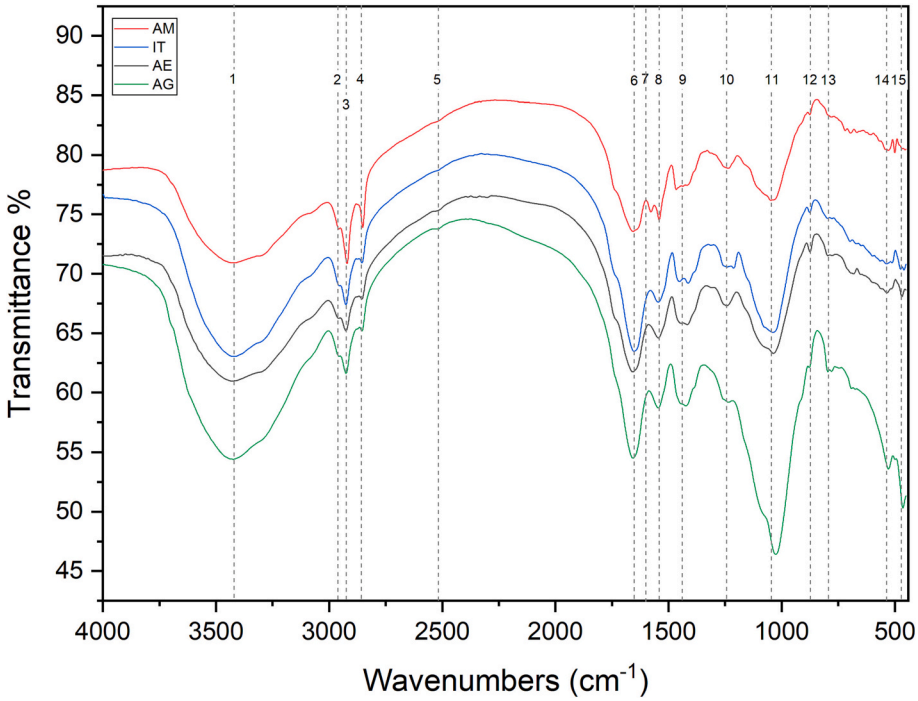

Fig. 2. FT-IR spectra of BS from AM, IT, AE, AG.

Table 2
Infrared spectra bands assignments of BS from FT-IR spectra.

	AM	IT	AE	AG	Vibration	Bond	Functional Type	Reference
1	3428	3420	3428	3432	Stretching	H-bands, OH groups	Hydroxyl groups in carboxylic groups, phenols, polysaccharides, saturated aliphatic species	(Chefetz et al., 2006; Medina-Herrera et al., 2020)
2	2955	2956	2962	2962	Stretching, asymmetric	C-H, -CH_2 and -CH_3	Fatty chains	(Chefetz et al., 2006)
3	2919	2924	2924	2931	Stretching asymmetric Vibration	C-H, CH_2	Alkyl C	(Fialho et al., 2010; Guibaud et al., 2003; Kang et al., 2007)
4	2852	2851	2853	2855	Stretching, symmetric, vibration	CH_2	Aliphatic methylene groups and assigned to fats & lipids	(Grube et al., 2006; Gulnaz et al., 2006; Wijesekara et al., 2018)
6	1656	1650	1657	1655	Stretching asymmetric vibration	C=C in aromatic structure, COO-, H-banded C=O	Amide I, peptidic band, protein origin, protein dominant, aromatic ring, ketones, aldehydes	(Chefetz et al., 2006; Grube et al., 2006; Kowalski et al., 2018)
7	1577	–	–	–	Deforming vibration	NH_2	Amide II	(Chefetz et al., 2006; Kowalski et al., 2018)
8	1541	1545	1548	1541		N-H bend	Protein origin, amide II	(Grube et al., 2006; Kang et al., 2007)
9	1466	1454	1424	1425	Stretching	O-H and C-O	Phenolic	(Gulnaz et al., 2006)
10	1235	1245	1247	1236	Stretching asymmetric, sharp band, deforming vibration	P=O, C-O-C, C=O	Amide III, fats, Lipopolysaccharides (LPS), nucleic acids, ribose	(Kang et al., 2007; Kowalski et al., 2018)
11	1035	1035	1035	1024	Stretching	C-H in plane, C-O	Minerals containing phosphates and silicates CH_2OH carbohydrates, polysaccharides	(Elakiya and Arulmozhiselvan, 2021; Quilès et al., 2010; Tapia et al., 2010)
12	878	880	877	880	Stretching vibrations	C-O, $Ca(OH)_2$	Polysaccharides and carbonate species	(Lü et al., 2018; Pullket, 2015)
13	778	802	800	800	Stretching	C-O	Carbonate	(Elakiya and Arulmozhiselvan, 2021)

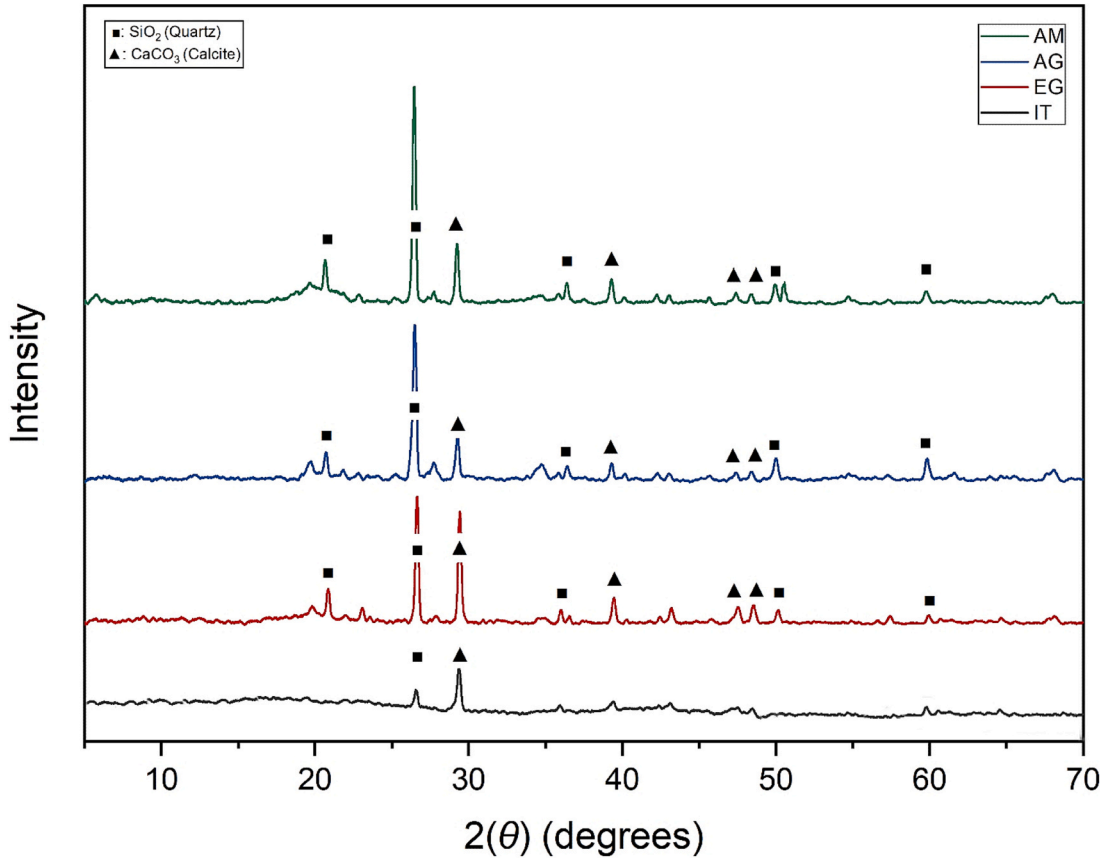

Fig. 3. Powder XRD patterns of BS from AM, IT, AE, AG. Data was obtained via DIFFRAC-EVA.

and the identification of the peaks revealed that the dominant part of the samples is the organic (Flores-Álvarez et al., 2011), confirming the TG analysis results. This part includes biodegradable molecules, such as carboxylic acids, lipids, proteins and aliphatic hydrocarbons and the recalcitrant molecules of cellulose and lignin, which are also present into their matrix. So, this knowledge of the composition of BS content in bioavailable organic matter is crucial because it is related to microbial activity and thus to the "bio stability" of BS as organic residues (Lü et al., 2018). In addition, the existence of positively or negatively charged functional groups such as amines and carboxylates, respectively, gives to BS the ability to adsorb anions and cations from a theoretical point of view (Kang et al., 2007). Therefore, the addition of BS to the soil makes it possible to bind metals by complexation or adsorption mechanisms, contributing to the remediation of polluted soils and preventing them from ending up in the underground aquifer (Lu et al., 2012).

3.5. Mineralogical crystalline phase of BS

XRD provided the mineralogical composition of the sampled BS. The X-ray diffraction patterns of the BS, are presented in Fig. 3. The patterns are qualitatively similar, although some differences in peak intensities are clearly noticed, but overall, sharp peaks are seen, indicative of the crystalline nature of the samples. Silicon dioxide (SiO_2) was detected as the main crystalline material in their structure, followed by calcium carbonate ($CaCO_3$) (Onchoke et al., 2018), All four patterns show peaks at $2\theta = 26.5^{\circ}$, which are attributed to SiO_2 with crystallite size varying from 58 nm to 65 nm. The peak of calcium carbonate ($CaCO_3$) at $2\theta = 29.2^{\circ}$ appears also in all four samples, with crystallite size from 43.2 nm to 55.8 nm, indicating better dispersion.

Since BS are neither fully crystalline nor amorphous, as we can see from the values of Table S5, the crystallinity is expressed in terms of a degree of crystallinity, which is a measure of extent to which the material can be considered as crystalline (Bishnoi et al., 2017). The amorphous part of BS is also confirmed through the SEM images.

3.6. Solid-state NMR spectroscopy of BS

Solid-state ^{13}C CPMAS NMR spectroscopy was performed additionally to FT-IR spectroscopy. For the comparative evaluation of the samples and the understanding of their structure, the degree of aromaticity was calculated from the following equation:

$$\text{Degree of aromaticity} = \frac{\text{aromatic C110} - \text{160 ppm}}{\text{aromatic C (110} - \text{160 ppm)} + \text{aliphatic C (0} - \text{110 ppm)}} * 100\% \quad (1)$$

(Piterina et al., 2009).

The organic carbon composition of the BS fraction evaluated by solid state NMR, revealed the chemical shifts characteristic for aliphatic C, O-substituted aliphatic C, aromatic C and carboxylic C (Fig. 4). Specifically, the intense resonances centered around 30 ppm refer to polyethylene chains found in simple lipids (e.g. alkanes, fatty acids, alcohols) and lipid polyesters. In the region of substituted aliphatic C the peaks included in the 45–60 ppm range may be assigned to C—N groups whereas the weak intensity of specific signatures related to lignin derivatives in phenolic region (145–160 ppm) suggested a lower presence of methoxyl groups O-CH_3, substituents in aromatic rings. The broad bands at 70 ppm are mainly associated to O-alkyl functions of polyhydroxyl components such as those of pyranose and furanose units of carbohydrates, while the signals shifted towards 100–105 ppm highlight the presence of di-O-alkyl O—CH—O groups typical of anomeric C involved in glycosidic linkage (Mao et al., 2003). The coexistence of these peaks in the spectrum indicates the presence of a large fraction of

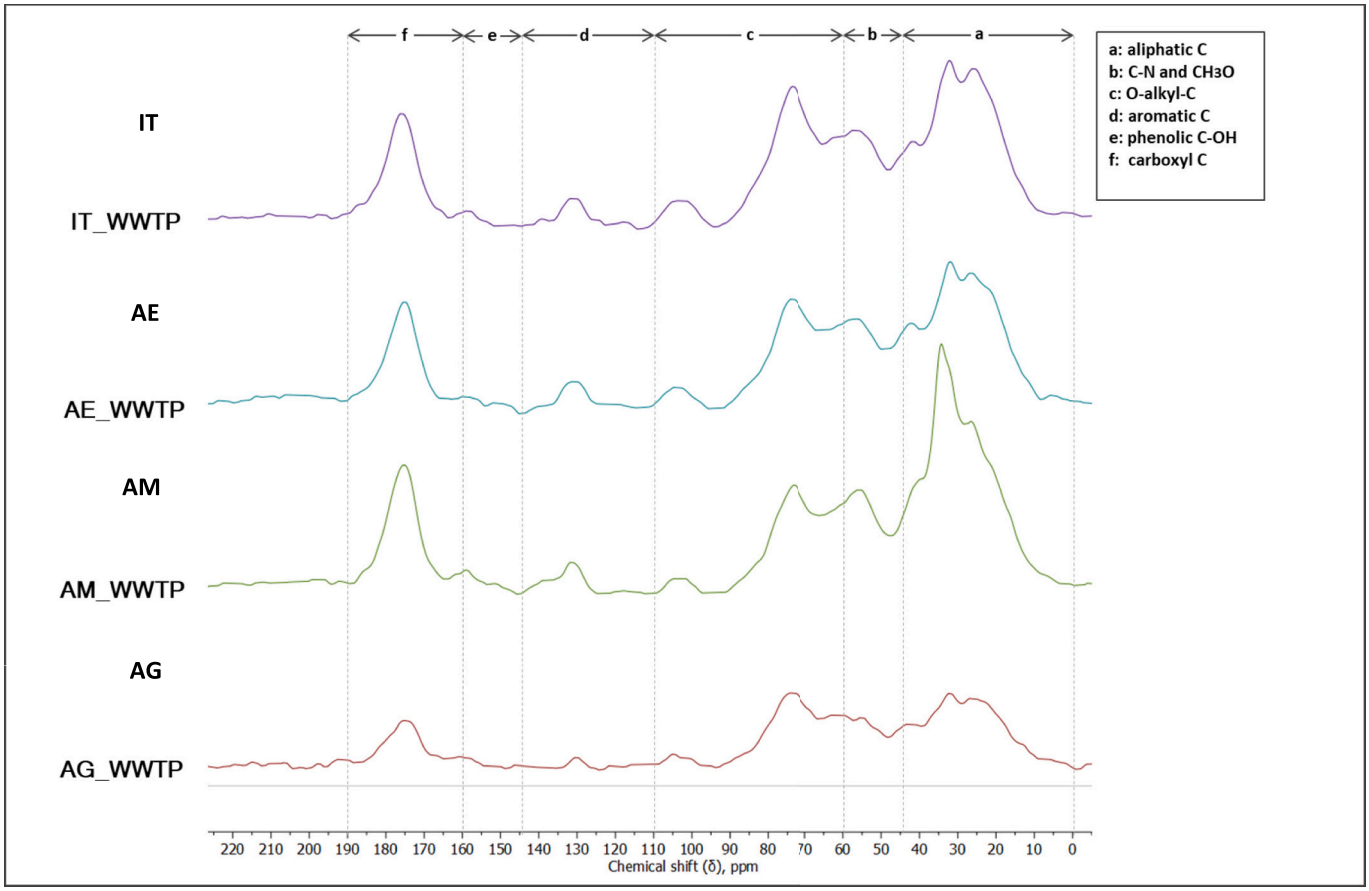

Fig. 4. Solid state 13C cross-polarization magic-angle-spinning NMR spectra of BS.

polysaccharides in the BS samples (Mao et al., 2003; Smernik et al., 2003). Less intense peaks were located in the aromatic region, with the chemical shift at 128 ppm being an indication of substituted or unsubstituted aromatic C. A high intensity peak occurs at a chemical shift of 173 ppm, due to the presence of carboxyl groups involved in amide and/or ester structures (Piterina et al., 2009). The lower degree of aromaticity which ranged from 7.7 to 11,4 % (Table S4) is attributed to the immaturity of the samples, in terms of their humification degree. This fact is due to the characterization of the samples immediately after their production in the WWTP. In case of storage of the BS or its further processing, its percentage of aromaticity would show an increase, due to the possible synthesis of the protein-rich, EPS components, by the present bacterial communities. The relative contribution of each functional group (Table S4) was determined by dividing the area of each spectral region by the sum of all spectral areas. It is observed that all samples are rich in aliphatic compounds (45–0 ppm) and carbohydrates derivatives (110–60 ppm) with a noticeable contribution of carboxylate (190–160 ppm) functions. A lower abundance was found for both phenolic and aromatic C (160–145 ppm, 145–100 ppm). The results follow literature records (Al-Faiyz, 2017; Chiu and Tian, 2011; Piterina et al., 2009; Rowell et al., 2001).

3.7. Fluorescence emission spectrum of BS DOM (EEM)

Fluorescence spectra can be quantified using various methods, depending on the specific application and the type of data to be extracted. In this case, the five-region separation according to Chen et al., 2003 (Chen et al., 2003) was followed, as shown in Table S5.

Region A (ex. 250–400 nm, em. 380–500 nm) relates to humic acid-like substances, region B (ex. 250–400 nm, em. 280–380 nm) refers to soluble microbial byproduct-like materials, region C (ex. 220–250 nm, em. 380–450 nm) usually associated with fulvic acid-like substances, and regions D and E (ex. 220–250 nm, em. 330–380 nm and 280–330 nm, respectively) involving proteins, such as tryptophan and tyrosine (Wang et al., 2013).

As shown in Fig. 5, AM has a strong microbial load (Region B) and is the only sample that showed intensities in all regions, i.e. B, C, D, E, which demonstrates a material with a rich organic matrix. Overall, it appears that humic acid-like organics were the dominant part of DOM in the aqueous extraction of all four samples. However, the maximum fluorescence intensity of AG, AM, AE (390–520 AU) differentiates IT which intensity is obviously lower (250 AU).

3.8. Morphological characteristics of BS surface

SEM/EDS analysis performed in order to study the morphological characteristics of the BS surface and provide additional information to ICP-OES. EDS spectra collected at different locations on each sample to identify the remaining elements. The EDS spectra show the presence of macro and micro elements (Na, K, Mg, Ca, Al, P, Si, Cl) of the BS. As for a representative sample for the elemental analysis was chosen the AE WWTP (Fig. S7). Heavy metals, such as: Pb, Cd, Co and Ni, were not

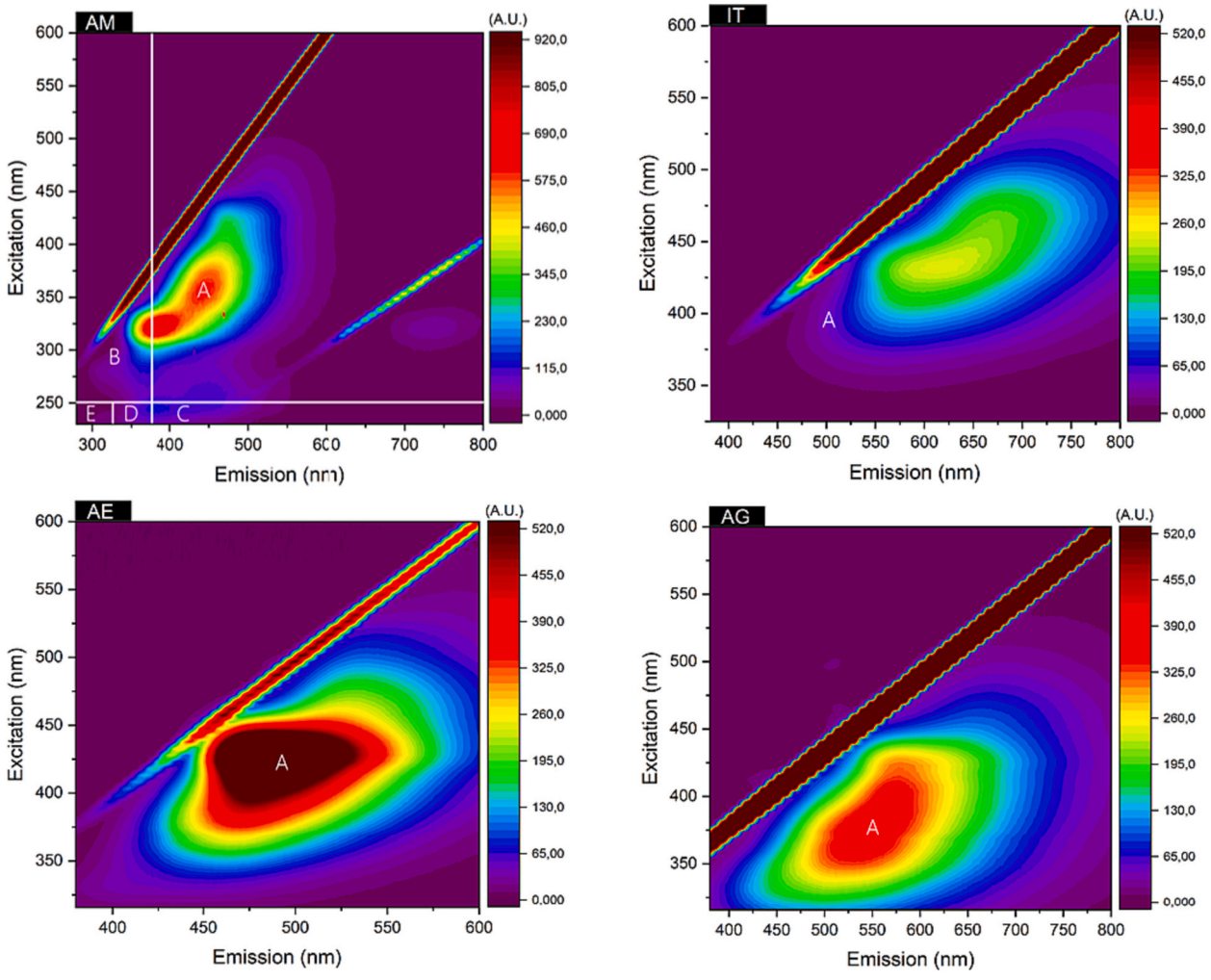

Fig. 5. EEM fluorescence spectra of DOM extracted from BS from different WWTPs, derived in the five-regions according to Chen et al., 2003.

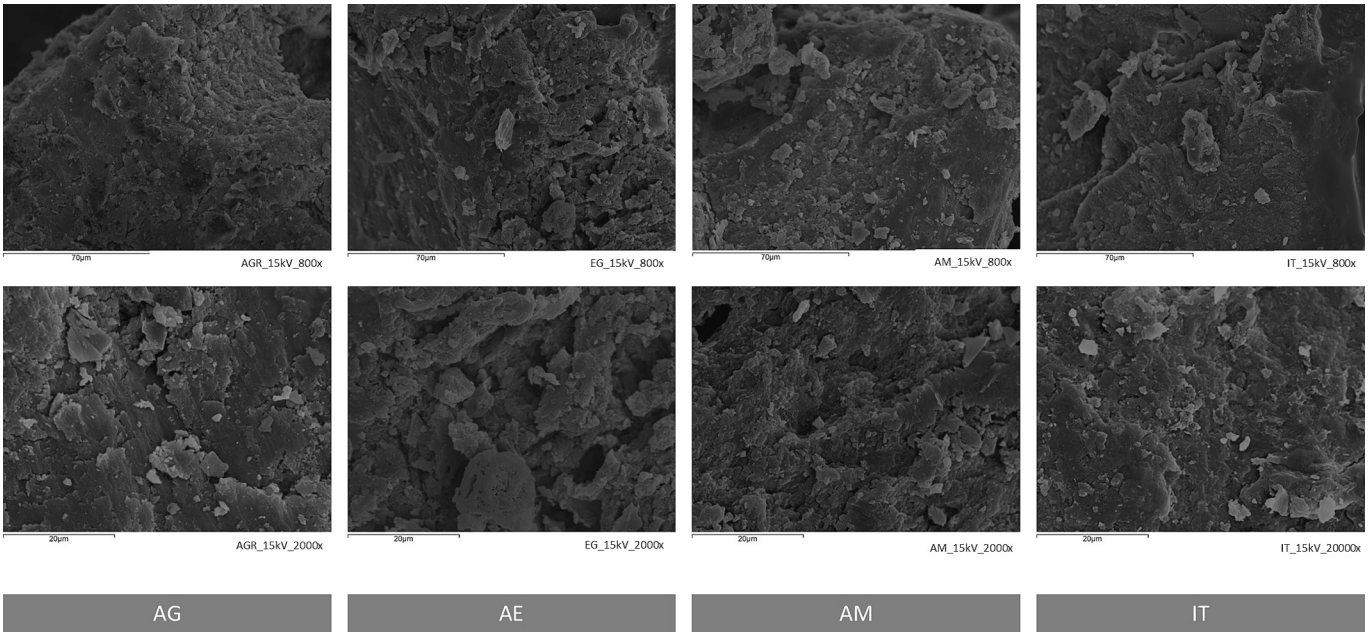

Fig. 6. SEM photographs showing the micro-porosity of the BS from the four processing units.

detectable using EDS, probably due to the spot analysis of this technique, in contrast to the ICP-OES results. Au was ignored, as it is attributed to the gold coated step of the sample preparation procedure. Spectrum peaks and detected elements follow the literature (Bolan et al., 2013; Onchoke et al., 2018; Roychand et al., 2021).

The surface of the samples shows a clear heterogeneity and follow a common pattern. Analysis of the SEM micrographs (Fig. 6) reveals that the BS are amorphous materials, with compact structure, which is in agreement with the rest of the studies (Kelly et al., 2020; Roychand et al., 2021). AE present larger particles with a diameter of ~20 μm and AG has smoother surface. The similarity of the SEM images is attributed probably to the fact that all the WWTPs undergo more or less similar processes of treatment (Table S1). The color difference in individual points probably represent a different composition of the materials.

4. Conclusions

The characterization of natural organic matter is the subject of many analytical techniques reported extended in literature. However, the complexity of its structure, and especially that of BS, is an obstacle to drawing clear conclusions about their exact composition. In the current study, the structural characterization of BS from four (4) WWTPs was studied by means of spectroscopic and analytical techniques. This proposed approach, demands expertise in terms of instrument handling and interpretation of their outputs. Nevertheless, this study contributes to literature with some comprehensive data of elemental composition, morphological pore sizes and chemical structure of these organic residues. BS have pH values close to seven (7) and conductivity permissible for their use as fertilizers or soil conditioners. In reference to the molecular composition of the samples, determined by FT-IR, Fluorescence and ^{13}C CP MAS NMR analysis, proved to be rich in organic matter, independent from the location of WWTPs or the treatment processes they have undergone. Eliminating the problem of their variability. In this way, BS application is independent of their origin. It is safe to state that the studied BS presented the same characteristic groups and were evaluated as materials with long aliphatic chains, and at a smaller percentage aromatic character. Their aromaticity may be attributed to humic substances, but their low concentration is a limitation for application in agriculture as soil amendments. On the contrary, they can be characterized as N-rich materials because of the existence of Organic-N in complex molecules such as proteins, nucleic acids, amines and other cellular materials, which can enhance soil fertility. SEM proved that BS are non-porous materials, which confirmed the findings of XRD analysis for a randomly amorphous structure. The inorganic load of the BS is of great importance, as the micro and macro-nutrients determined are in permissible concentrations, allowing their use as possible mineral fertilizers in alkaline and sandy soils. In this way, they enhance the bioremediation process as they provide microorganisms with the necessary food to grow and consequently degrade organic matter, including emerging organic pollutants. Another challenging study complementary to the present one in the context of estimating the degree of BS suitability for industrial and agricultural applications beyond pathogen load, is the detection of emerging pollutants, such as pharmaceuticals or microplastics.

Supplementary data to this article can be found online at https://doi.org/10.1016/j.scitotenv.2023.168425.

CRediT authorship contribution statement

E.I. conceived of the presented idea. A.K. set the contents and defined the analyzed sequence data of the research. I.K. determined the wastewater treatment plants of research and supervised this manuscript. I.Z., C.S. and B.A. conducted the experiments and contributed with their knowledge to the XRD, NMR and metal analysis, respectively. A.K. wrote the manuscript with support from E.I. All authors discussed the results and contributed to the final manuscript.

Declaration of competing interest

The authors declare that they have no known competing financial interests or personal relationships that could have appeared to influence the work reported in this paper.

Data availability

Data will be made available on request.

Acknowledgements

The authors fully acknowledge the technical support provided by Katerina Govatsi of the Laboratory of Electron Microscopy and Micro-analysis (LEMM) at University of Patras for SEM images. The team wishes to thank the WWTPs facility personnel who contributed to the survey by providing the BS samples, i.e. Christoforo Kostaki and Kosta Dania (Agrinio WWTP), Panagioti Nikolopoulo (Aegio WWTP), Ioanni Nikaki and Niko Apostolopoulo (Amaliada WWTP) and Ilia Dimitrello (ITEA WWTP).

References

Aadraoui, M., Elbaghdadi, M., Rais, J., Barakat, A., W., E., Karroum, L. A., & Oumenskoual, H., 2017. Effect of incineration of sewage sludge on the evolution of physicochemical characterization and mineralogical properties. J. Mater. Environ. Sci. 8 (8), 2800–2806. https://www.jmaterenvironsci.com/Document/vol8/vol8_N8/299-JMES-Aadraoui.pdf.

Aguilera, S.M., Borie, G., Peirano, P., Rodriguez, M., Grez, I., Zunino, H., 2007. Chemical characterization of sewage sludges in Chile and their potential utilization as amendment to reclaim soils for forestation purposes. J. Plant Nutr. 30 (12), 1993–2003. https://doi.org/10.1080/01904160701700400.

Al-Faiyz, Y.S.S., 2017. CPMAS 13 C NMR characterization of humic acids from composted agricultural Saudi waste. Arab. J. Chem. 10, S839–S853. https://doi.org/10.1016/j.arabjc.2012.12.018.

Bishnoi, A., Kumar, S., Joshi, N., 2017. Wide-angle X-ray diffraction (WXRD). In: Microscopy Methods in Nanomaterials Characterization. Elsevier, pp. 313–337. https://doi.org/10.1016/B978-0-323-46141-2.00009-2.

Bolan, N.S., Kunhikrishnan, A., Naidu, R., 2013. Carbon storage in a heavy clay soil landfill site after biosolid application. Sci. Total Environ. 465, 216–225. https://doi.org/10.1016/j.scitotenv.2012.12.093.

Carrasquero-Durán, A., Flores, I., 2009. Evaluation of lead(II) immobilization by a vermicompost using adsorption isotherms and IR spectroscopy. Bioresour. Technol. 100 (4), 1691–1694. https://doi.org/10.1016/J.BIORTECH.2008.09.013.

Chaudhary, Heidi L., Y. K. G., 2021. Identifying ranges of combined lime and heat treatments to achieve biosolids stabilization fecal coliform targets. J. Environ. Manage. 282 (NA) https://doi.org/10.1016/j.jenvman.2020.111900, 111900-NA.

Chefetz, B., Ilani, T., Schulz, E., Chorover, J., 2006. Wastewater dissolved organic matter: characteristics and sorptive capabilities. Water Sci. Technol. 53 (7), 51–57. https://doi.org/10.2166/WST.2006.207.

Chen, X., Jeyaseelan, S., 2001. Study of sewage sludge pyrolysis mechanism and mathematical modeling. J. Environ. Eng. 127 (7), 585–593. https://doi.org/10.1061/(ASCE)0733-9372(2001)127:7(585).

Chen, W., Westerhoff, P., Leenheer, J.A., Booksh, K., 2003. Fluorescence excitation−emission matrix regional integration to quantify spectra for dissolved organic matter. Environ. Sci. Technol. 37 (24), 5701–5710. https://doi.org/10.1021/es034354c.

Chiu, C.Y., Tian, G., 2011. Chemical structure of humic acids in biosolids-amended soils as revealed by NMR spectroscopy. Appl. Soil Ecol. 49 (1), 76–80. https://doi.org/10.1016/j.apsoil.2011.06.013.

Collivignarelli, M.C., Canato, M., Abbà, A., Carnevale Miino, M., 2019. Biosolids: what are the different types of reuse? J. Clean. Prod. 238, 117844 https://doi.org/10.1016/j.jclepro.2019.117844.

Collivignarelli, M.C., Abbà, A., Benigna, I., 2020. The reuse of biosolids on agricultural land: critical issues and perspective. Water Environ. Res. 92 (1), 11–25. https://doi.org/10.1002/wer.1196.

Demirbas, A., Edris, G., Alalayah, W.M., 2017. Sludge production from municipal wastewater treatment in sewage treatment plant. Energy Sources, Part A 39 (10), 999–1006. https://doi.org/10.1080/15567036.2017.1283551.

Demitrelos, E., Koukoulakis, P.H., Kyritsis, S.S., Bountla, A., Isari, E., Kalavrouziotis, I.K., 2022. Impact of elemental interactions on soil metal availability and growth of ryegrass (Lolium perenne L.) under wastewater and biosolids. Water Air Soil Pollut. 233 (3), 96. https://doi.org/10.1007/s11270-022-05561-5.

DEP, 2021. Sludge Sampling and Analytical Guidance Document. New Jersey Department of Environmental Protection Division of Water Quality Bureau of Ground Water, Residuals and Permit Administration. https://www.nj.gov/dep/dwq/pdf/final_njssag_doc.pdf.

DIFFRAC EVA (No. 2008). (n.d.). BrukerAXS.

Elakiya, N., Arulmozhiselvan, K., 2021. Characterization of substrates of growing media by fourier transform infrared (Ft-ir) spectroscopy for containerized crop production. *Journal of Applied and Natural*. Science 13 (SI), 35–42. https://doi.org/10.31018/jans.v13iSI.2774.

European Union, 1986. Directive 86/278/EEC. http://data.europa.eu/eli/dir/1986/278/oj.

Fialho, L.L., da Silva, W.T.L., Milori, D.M.B.P., Simões, M.L., Martin-Neto, L., 2010. Characterization of organic matter from composting of different residues by physicochemical and spectroscopic methods. Bioresour. Technol. 101 (6), 1927–1934. https://doi.org/10.1016/J.BIORTECH.2009.10.039.

Flores-Álvarez, J.M., González, I., García-de la Rosa, L.A., Mancilla-Peña, F., Reyes-Gómez, J., 2011. Carbon paste electrodes modified with biosolids, soils and biocomposites utilized to study the interaction between organic matter and copper. J. Environ. Manage. 92 (3), 448–456. https://doi.org/10.1016/j.jenvman.2010.08.033.

Gao, N., Li, J., Qi, B., Li, A., Duan, Y., Wang, Z., 2014. Thermal analysis and products distribution of dried sewage sludge pyrolysis. J. Anal. Appl. Pyrolysis 105, 43–48. https://doi.org/10.1016/j.jaap.2013.10.002.

Garrido, S., Del Campo, G.M., Esteller, M.V., Vaca, R., Lugo, J., 2005. Heavy metals in soil treated with sewage sludge composting, their effect on yield and uptake of broad bean seeds (Vicia faba L.). Water Air Soil Pollut. 166 (1–4), 303–319. https://doi.org/10.1007/s11270-005-5269-4.

Giannakopoulos, E., Kalavrouziotis, I.K., Dimitrelos, H., Koukoulakis, P.H., Varnavas, S. P., Papadopoulos, F., 2017. Evaluation of interactions among sewage sludge bioavailable metals from WWTPs using DTPA agent. Desalin. Water Treat. 71, 25–31. https://doi.org/10.5004/dwt.2017.20436.

Grube, M., Lin, J.G., Lee, P.H., Kokorevicha, S., 2006. Evaluation of sewage sludge-based compost by FT-IR spectroscopy. Geoderma 130 (3–4), 324–333. https://doi.org/10.1016/J.GEODERMA.2005.02.005.

Guibaud, G., Tixier, N., Bouju, A., Baudu, M., 2003. Relation between extracellular polymers' composition and its ability to complex cd. Cu and Pb. Chemosphere 52 (10), 1701–1710. https://doi.org/10.1016/S0045-6535(03)00355-2.

Gulnaz, O., Kaya, A., Dincer, S., 2006. The reuse of dried activated sludge for adsorption of reactive dye. J. Hazard. Mater. 134 (1–3), 190–196. https://doi.org/10.1016/J.JHAZMAT.2005.10.050.

Ho, C.P., Yuan, S.T., Jien, S.H., Hseu, Z.Y., 2010a. Elucidating the process of co-composting of biosolids and spent activated clay. Bioresour. Technol. 101 (21), 8280–8286. https://doi.org/10.1016/j.biortech.2010.06.058.

Ho, C.P., Yuan, S.T., Jien, S.H., Hseu, Z.Y., 2010b. Elucidating the process of co-composting of biosolids and spent activated clay. Bioresour. Technol. 101 (21), 8280–8286. https://doi.org/10.1016/J.BIORTECH.2010.06.058.

Hossner, L.R., 2018. Dissolution for Total Elemental Analysi, pp. 49–64. https://doi.org/10.2136/sssabookser5.3.c3.

Jan, M.H., H., Jon M, W., Dennis L, C., R, G.K., 2018. 6.1 Solute Content and Concentration, pp. 1253–1321. https://doi.org/10.2136/sssabookser5.4.c54.

Kalavrouziotis, I.K., 2016. In: Eslamian, S. (Ed.), Urban Water Reuse Handbook, 1st Editio. CRC Press. https://doi.org/10.1201/b19646.

Kalavrouziotis, I.K., Koukoulakis, P., 2016. EQA – Environmental quality / Qualité de l'Environnement / Qualità ambientale, 20 (2016), 1–13, 20, 1–13. https://doi.org/10.6092/issn.2281-4485/6303.

Kang, S.-Y., Kim, D.-W., Kim, K.-W., 2007. Enhancement of As(V) adsorption onto activated sludge by methylation treatment. Environ. Geochem. Health 29 (4), 313–318. https://doi.org/10.1007/s10653-007-9096-y.

Kanteraki, A.E., Isari, E.A., Svarnas, P., Kalavrouziotis, I.K., 2022. Biosolids: the Trojan horse or the beautiful Helen for soil fertilization? Sci. Total Environ. 839, 156270 https://doi.org/10.1016/j.scitotenv.2022.156270.

Kelly, J.E., Chrissian, C., Stark, R.E., 2020. Tailoring NMR experiments for structural characterization of amorphous biological solids: A practical guide. Solid State Nucl. Magn. Reson. 109, 101686 https://doi.org/10.1016/J.SSNMR.2020.101686.

Kowalski, M., Kowalska, K., Wiszniowski, J., Turek-Szytow, J., 2018. Qualitative analysis of activated sludge using FT-IR technique. 72, 2699–2706. https://doi.org/10.1007/s11696-018-0514-7.

Laidlaw, W.S., Baker, A.J.M., Gregory, D., Arndt, S.K., 2015. Irrigation water quality influences heavy metal uptake by willows in biosolids. J. Environ. Manage. 155 (NA), 31–39. https://doi.org/10.1016/j.jenvman.2015.03.005.

Li, W., Zhou, R., Zhou, R., Weerasinghe, J., Zhang, T., Gissibl, A., Cullen, P.J., Speight, R., Ostrikov, K., (Ken)., 2022. Insights into amoxicillin degradation in water by non-thermal plasmas. Chemosphere 291, 132757. https://doi.org/10.1016/j.chemosphere.2021.132757.

Lindsay, W.L., Norvell, W.A., 1978. Development of a DTPA soil test for zinc, Iron, manganese, and copper. Soil Sci. Soc. Am. J. 42 (3), 421–428. https://doi.org/10.2136/sssaj1978.03615995004200030009x.

Lu, Q., He, Z.L., Stoffella, P.J., 2012. Land application of biosolids in the USA: a review. Appl. Environ. Soil Sci. 2012 (NA), 1–11. https://doi.org/10.1155/2012/201462.

Lü, F., Shao, L.-M., Zhang, H., Fu, W.-D., Feng, S.-J., Zhan, L.-T., Chen, Y.-M., He, P.-J., 2018. Application of advanced techniques for the assessment of bio-stability of biowaste-derived residues: a minireview. Bioresour. Technol. 248, 122–133. https://doi.org/10.1016/j.biortech.2017.06.045.

Mao, J.-D., Hundal, L.S., Schmidt-Rohr, K., Thompson, M.L., 2003. Nuclear magnetic resonance and diffuse-reflectance infrared Fourier transform spectroscopy of biosolids-derived biocolloidal organic matter. Environ. Sci. Technol. 37 (9), 1751–1757. https://doi.org/10.1021/es020821z.

Martínez, E.J., Fierro, J., Sánchez, M.E., Gómez, X., 2012. Anaerobic co-digestion of FOG and sewage sludge: study of the process by Fourier transform infrared spectroscopy. Int. Biodeter. Biodegr. 75, 1–6. https://doi.org/10.1016/J.IBIOD.2012.07.015.

Mattigod, S.V., Zachara, J.M., 1996. Methods of Soil Analysis. In: Sparks, D.L., Page, A.L., Helmke, P.A., Loeppert, R.H., Soltanpour, P.N., Tabatabai, M.A., Johnston, C.T., Sumner, M.E. (Eds.), Methods of soil analysis. Soil Science Society of America, American Society of Agronomy. https://doi.org/10.2136/sssabookser5.3.

Medina-Herrera, M. del R., Negrete-Rodríguez, M. de la L. X., Álvarez-Trejo, J. L., Samaniego-Hernández, M., González-Cruz, L., Bernardino-Nicanor, A., Conde-Barajas, E., 2020. Evaluation of non-conventional biological and molecular parameters as potential indicators of quality and functionality of urban biosolids used as organic amendments of agricultural soils. Appl. Sci. 10 (2), 517. https://doi.org/10.3390/app10020517.

Mossa, A.-W., Dickinson, M.J., West, H.M., Young, S.D., Crout, N.M.J., 2017. The response of soil microbial diversity and abundance to long-term application of biosolids. Environ. Pollut. 224 (NA), 16–25. https://doi.org/10.1016/j.envpol.2017.02.056.

Mymrin, V., Hackbart, F.M., Alekseev, K., Avanci, M.A., Winter, E., Marinho, G.P., Iarozinski, N., A., & Catai, R. E., 2019. Construction materials wastes use to neutralize hazardous municipal water treatment sludge. Construct. Build Mater. 204, 800–808. https://doi.org/10.1016/j.conbuildmat.2019.01.182.

Office Of Water, 1969. Sludge Sampling And Analysis Guidance Document. In: United States Environmental Protection Agency, pp. 2–22. https://www.epa.gov/sites/default/files/2018-11/documents/potw-sludge-sampling-guidance-document.pdf.

Onchoke, K.K., Franclemont, C.M., Weatherford, P.W., 2018. Structural characterization and evaluation of municipal wastewater sludge (biosolids) from two rural wastewater treatment plants in East Texas, USA. Spectrochim. Acta A Mol. Biomol. Spectrosc. 204, 514–524. https://doi.org/10.1016/j.saa.2018.06.096.

Patel, S.R., Kundu, S.K., Halder, P.K., Setiawan, A., Paz-Ferreiro, J., Surapaneni, A., Shah, K.V., 2018. A hybrid kinetic analysis of the biosolids pyrolysis using thermogravimetric analyser. ChemistrySelect 3 (47), 13400–13407. https://doi.org/10.1002/slct.201802957.

Paz-Ferreiro, J., Nieto, A., Méndez, A., Askeland, M., Gascó, G., 2018. Biochar from biosolids pyrolysis: a review. Int. J. Environ. Res. Public Health 15 (5), 956. https://doi.org/10.3390/ijerph15050956.

Piterina, A., Barlett, J., Pembroke, J.T., 2009. 13C-NMR assessment of the pattern of organic matter transformation during domestic wastewater treatment by autothermal aerobic digestion (ATAD). Int. J. Environ. Res. Public Health 6 (8), 2288–2306. https://doi.org/10.3390/ijerph6082288.

Pollice, A., Giordano, C., Laera, G., Saturno, D., Mininni, G., 2007. Physical characteristics of the sludge in a complete retention membrane bioreactor. Water Res. 41 (8), 1832–1840. https://doi.org/10.1016/j.watres.2007.01.022.

Pullket, S., 2015. Sewage Sludge as Source of Activated Carbon for the Removal of Endocrine Disrupting Chemicals in Wastewater.

Quilès, F., Humbert, F., Delille, A., 2010. Analysis of changes in attenuated total reflection FTIR fingerprints of Pseudomonas fluorescens from planktonic state to nascent biofilm state. Spectrochim. Acta A Mol. Biomol. Spectrosc. 75 (2), 610–616. https://doi.org/10.1016/J.SAA.2009.11.026.

Ravindran, B., Dinesh, S.L., Kennedy, L.J., Sekaran, G., 2008. Vermicomposting of Solid Waste Generated from Leather Industries Using Epigeic Earthworm *Eisenia foetida*. https://doi.org/10.1007/s12010-008-8222-3.

Rowell, D.M., Prescott, C.E., Preston, C.M., 2001. Decomposition and nitrogen mineralization from biosolids and other organic materials: relationship with initial chemistry. J. Environ. Qual. 30 (4), 1401–1410. https://doi.org/10.2134/jeq2001.3041401x.

Roychand, R., Patel, S., Halder, P., Kundu, S., Hampton, J., Bergmann, D., Surapaneni, A., Shah, K., Pramanik, B.K., 2021. Recycling biosolids as cement composites in raw, pyrolyzed and ashed forms: a waste utilisation approach to support circular economy. J. Build. Eng. 38, 102199 https://doi.org/10.1016/j.jobe.2021.102199.

Senesi, N., Miano, T.M., Provenzano, M.R., Brunetti, G., 1991. Characterization, differentiation, and classification of humic substances by fluorescence spectroscopy. Soil Sci. 152 (4), 259–271. https://doi.org/10.1097/00010694-199110000-00004.

Sharma, B., Sarkar, A., Singh, P., Singh, R.P., 2017. Agricultural utilization of biosolids: a review on potential effects on soil and plant grown. Waste Manag. 64, 117–132. https://doi.org/10.1016/j.wasman.2017.03.002.

Silveira, M., Alleoni, L., Guilherme, L., 2003. Biosolids and heavy metals in soils. Sci. Agric. 60 (4), 793–806. https://doi.org/10.1590/S0103-90162003000400029.

Silveira, M.L., Chang, A.C., Alleoni, L.R.F., O'Connor, G.A., Berton, R., 2007. Metal-associated forms and speciation in biosolid-amended oxisols. Commun. Soil Sci. Plant Anal. 38 (7–8), 851–869. https://doi.org/10.1080/00103620701263700.

Smernik, R.J., Oliver, I.W., Merrington, G., 2003. Characterization of sewage sludge organic matter using solid-state carbon-13 nuclear magnetic resonance spectroscopy. J. Environ. Qual. 32 (4), 1516. https://doi.org/10.2134/jeq2003.1516.

Smidt, E., Meissl, K., 2007. The applicability of Fourier transform infrared (FT-IR) spectroscopy in waste management. Waste Manag. 27 (2), 268–276. https://doi.org/10.1016/j.wasman.2006.01.016.

Smith, S.R., 2008. FINAL REPORT FOR DISCUSSION The Implications for Human Health and the Environment of Recycling Biosolids on Agricultural Land. http://www3.imperial.ac.uk/ewre.

Svarnas, P., Giannakopoulos, E., Kalavrouziotis, I., Krontiras, C., Georga, S., Pasolari, R. S., Papadopoulos, P.K., Apostolou, I., Chrysochoou, D., 2020. Sanitary effect of FE-DBD cold plasma in ambient air on sewage biosolids. Sci. Total Environ. 705 (NA), 135940 https://doi.org/10.1016/j.scitotenv.2019.135940.

Tapia, Y., Cala, V., Eymar, E., Frutos, I., Gárate, A., Masaguer, A., 2010. Chemical characterization and evaluation of composts as organic amendments for immobilizing cadmium. Bioresour. Technol. 101 (14), 5437–5443. https://doi.org/10.1016/j.biortech.2010.02.034.

Thomas, G.W., 2018. Soil pH and Soil Acidity, pp. 475–490. https://doi.org/10.2136/sssabookser5.3.c16.

Vochozka, M., Maroušková, A., Váchal, J., Straková, J., 2016. Advances in economically driven optimization of processing of biosolids from sewage sludge. Energy Sources, Part A 38 (16), 2413–2417. https://doi.org/10.1080/15567036.2015.1084404.

Walker, J.M., Knight, L., Stein, L., Management, U.S.E.P.A.O., of W, 1994. A Plain English Guide to the EPA Part 503 Biosolids Rule. U.S. Environmental Protection Agency, Office of Wastewater Management Washington, DC, In TA - TT doi:https://worldcat.org/title/32057388.

Wang, K., Li, W., Gong, X., Li, Y., Wu, C., Ren, N., 2013. Spectral study of dissolved organic matter in biosolid during the composting process using inorganic bulking agent: UV–vis, GPC, FTIR and EEM. Int. Biodeter. Biodegr. 85, 617–623. https://doi.org/10.1016/j.ibiod.2013.03.033.

Wang, X., Andrade, N., Shekarchi, J., Fischer, S.J., Torrents, A., Ramirez, M., 2018. Full scale study of Class A biosolids produced by thermal hydrolysis pretreatment and anaerobic digestion. Waste Manag. 78 (NA), 43–50. https://doi.org/10.1016/j.wasman.2018.05.026.

Wijesekara, H., Bolan, N.S., Bradney, L., Obadamudalige, N., Seshadri, B., Kunhikrishnan, A., Dharmarajan, R., Ok, Y.S., Rinklebe, J., Kirkham, M.B., Vithanage, M., 2018. Trace element dynamics of biosolids-derived microbeads. Chemosphere 199, 331–339. https://doi.org/10.1016/J.CHEMOSPHERE.2018.01.166.